

Fourier Neural Operator for Parametric Partial Differential Equations

Zongyi Li*, Nikola Kovachki*, Kamyar Azizzadenesheli†, Burigede Liu*,
Kaushik Bhattacharya*, Andrew Stuart*, Anima Anandkumar*

October 20, 2020

Abstract

The classical development of neural networks has primarily focused on learning mappings between finite-dimensional Euclidean spaces. Recently, this has been generalized to neural operators that learn mappings between function spaces. For partial differential equations (PDEs), neural operators directly learn the mapping from any functional parametric dependence to the solution. Thus, they learn an entire family of PDEs, in contrast to classical methods which solve one instance of the equation. In this work, we formulate a new neural operator by parameterizing the integral kernel directly in Fourier space, allowing for an expressive and efficient architecture. We perform experiments on Burgers’ equation, Darcy flow, and the Navier-Stokes equation (including the turbulent regime). Our Fourier neural operator shows state-of-the-art performance compared to existing neural network methodologies and it is up to three orders of magnitude faster compared to traditional PDE solvers.

1 Introduction

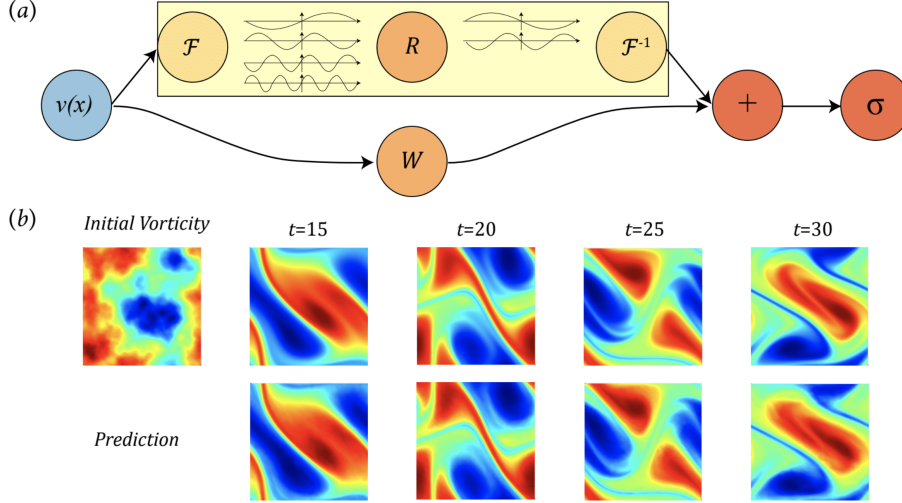
Many problems in science and engineering involve solving complex partial differential equation (PDE) systems repeatedly for different values of some parameters. Examples arise in molecular dynamics, micro-mechanics, and turbulent flows. Often such systems requires fine discretization in order to capture the phenomenon being modeled. As a consequence, traditional finite element methods (FEM) and finite difference methods (FDM) are slow and sometimes inefficient. For example, when designing materials such as airfoils, one needs to solve the associated inverse problem where thousands of evaluations of the forward model are needed. A fast method can make such problems feasible.

Machine learning methods hold the key to revolutionizing many scientific disciplines by providing fast solvers that approximate traditional ones. However, classical neural networks map between finite-dimensional spaces and can therefore only learn solutions tied to a specific discretization. This is often an insurmountable limitation for practical applications and therefore the development of mesh-invariant neural networks is required. We first outline two mainstream neural network based approaches for PDEs – the finite-dimensional operators and neural FEM.

Finite-dimensional operators. These approaches parameterize the solution operator as a deep convolutional neural network between finite-dimensional Euclidean spaces [Guo et al., 2016, Zhu and Zabaras, 2018, Adler and Oktem, 2017, Bhatnagar et al., 2019, Khoo et al., 2017]. Such approaches are, by definition, not mesh independent and will need modifications and tuning for different resolutions and discretizations in order to achieve consistent error (if at all possible). Furthermore, these approaches are limited to the discretization size and geometry of the training data and hence, it is not possible to query solutions at new points in the domain. In contrast, we show, for our method, both invariance of the error to grid resolution, and the ability to transfer the solution between meshes.

*Caltech, {zongyili, nkovachki, bgl, bhatta, astuart, anima}@caltech.edu

†Purdue University, kamyar@purdue.edu



(a) Start from input v . On top: apply the Fourier transform \mathcal{F} ; a linear transform R on the lower Fourier modes and filters out the higher modes; then apply the inverse Fourier transform \mathcal{F}^{-1} . On bottom: apply a local linear transform W . (b) Navier-Stokes Equation with Reynolds number 10,000; Ground truth on top and prediction on bottom; trained on $64 \times 64 \times 20$ dataset; evaluated on $256 \times 256 \times 80$ (see Section 5.3).

Figure 1: **top**: The architecture of the Fourier layer; **bottom**: Example flow from Navier-Stokes.

Neural-FEM. The second approach directly parameterizes the solution function as a neural network [E and Yu, 2018, Raissi et al., 2019, Bar and Sochen, 2019, Smith et al., 2020]. This approach is designed to model one specific instance of the PDE, not the solution operator. It is mesh-independent and accurate, but for any given new instance of the functional parameter/coefficient, it requires training a new neural network. The approach closely resembles classical methods such as finite elements, replacing the linear span of a finite set of local basis functions with the space of neural networks. The Neural-FEM approach suffers from the same computational issue as classical methods: the optimization problem needs to be solved for every new instance. Furthermore, the approach is limited to a setting in which the underlying PDE is known.

Neural Operators. Recently, a new line of work proposed learning mesh-free, infinite-dimensional operators with neural networks [Lu et al., 2019, Bhattacharya et al., 2020, Nelsen and Stuart, 2020, Li et al., 2020b, Li et al., 2020a]. The neural operator remedies the mesh-dependent nature of the finite-dimensional operator methods discussed above by producing a single set of network parameters that may be used with different discretizations. It has the ability to transfer solutions between meshes. Furthermore, the neural operator needs to be trained only once. Obtaining a solution for a new instance of the parameter requires only a forward pass of the network, alleviating the major computational issues incurred in Neural-FEM methods. Lastly, the neural operator requires no knowledge of the underlying PDE, only data. Thus far, neural operators have not yielded efficient numerical algorithms that can parallel the success of convolutional or recurrent neural networks in the finite-dimensional setting due to the cost of evaluating integral operators. Through the fast Fourier transform, our work alleviates this issue.

Fourier Transform. The Fourier transform is frequently used in spectral methods for solving differential equations, since differentiation is equivalent to multiplication in the Fourier domain. Fourier transforms have also played an important role in the development of deep learning. In theory, they appear in the proof of the universal approximation theorem [Hornik et al., 1989] and, empirically, they have been used to speed up convolutional neural networks [Mathieu et al., 2013]. Neural network architectures involving the Fourier transform or the use of sinusoidal activation functions have also been proposed and studied [Bengio et al., 2007, Mingo et al., 2004, Sitzmann et al., 2020]. Recently, some spectral methods for PDEs have been extended to neural networks [Fan et al., 2019a, Fan et al., 2019b]. We build on these works by proposing a neural operator architecture defined directly in Fourier space with quasi-linear time complexity

and state-of-the-art approximation capabilities.

Our Contributions. We introduce the Fourier neural operator, a novel deep learning architecture able to learn mappings between infinite-dimensional spaces of functions; the integral operator is instantiated through a linear transformation in the Fourier domain as shown in Figure 1 (a).

- By construction, the method shares the same learned network parameters irrespective of the discretization used on the input and output spaces for the purposes of computation.
- The proposed Fourier neural operator consistently outperforms all existing deep learning methods for parametric PDEs. It achieves error rates that are 30% lower on Burgers’ Equation, 60% lower on Darcy Flow, and 30% lower on Navier Stokes (turbulent regime with Reynolds number 10000) (Figure 1 (b)). When learning the mapping for the entire time series, the method achieves $< 1\%$ error with Reynolds number 1000 and 8% error with Reynolds number 10000.
- On a 256×256 grid, the Fourier neural operator has an inference time of only 0.005s compared to the 2.2s of the pseudo-spectral method used to solve Navier-Stokes. Despite its tremendous speed advantage, it does not suffer from accuracy degradation when used in downstream applications such as solving Bayesian inverse problem, as shown in Figure 3.

We observe that the Fourier neural operator captures global interactions through convolution with low-frequency functions and returns high-frequency modes by composition with an activation function, allowing it to approximate functions with slow Fourier mode decay (Section 5). Furthermore, local neural networks fix the periodic boundary which comes from the inverse Fourier transform and allows the method to approximate function with any boundary conditions. We demonstrate this by having non-periodic boundary on the spatial domain of Darcy flow and the time domain of Navier-Stokes equation.

2 Learning Operators

Our methodology learns a mapping between two infinite dimensional spaces from a finite collection of observed input-output pairs. Let $D \subset \mathbb{R}^d$ be a bounded, open set and $\mathcal{A} = \mathcal{A}(D; \mathbb{R}^{d_a})$ and $\mathcal{U} = \mathcal{U}(D; \mathbb{R}^{d_u})$ be separable Banach spaces of function taking values in \mathbb{R}^{d_a} and \mathbb{R}^{d_u} respectively. Furthermore let $G^\dagger : \mathcal{A} \rightarrow \mathcal{U}$ be a (typically) non-linear map. We study maps G^\dagger which arise as the solution operators of parametric PDEs – see Section 5 for examples. Suppose we have observations $\{a_j, u_j\}_{j=1}^N$ where $a_j \sim \mu$ is an i.i.d. sequence from the probability measure μ supported on \mathcal{A} and $u_j = G^\dagger(a_j)$ is possibly corrupted with noise. We aim to build an approximation of G^\dagger by constructing a parametric map

$$G : \mathcal{A} \times \Theta \rightarrow \mathcal{U} \tag{1}$$

or equivalently

$$G_\theta : \mathcal{A} \rightarrow \mathcal{U}, \quad \theta \in \Theta \tag{2}$$

for some finite-dimensional parameter space Θ by choosing $\theta^\dagger \in \Theta$ so that $G(\cdot, \theta^\dagger) = G_{\theta^\dagger} \approx G^\dagger$. This is a natural framework for learning in infinite-dimensions as one could define a cost functional $C : \mathcal{U} \times \mathcal{U} \rightarrow \mathbb{R}$ and seek a minimizer of the problem

$$\min_{\theta \in \Theta} \mathbb{E}_{a \sim \mu} [C(G(a, \theta), G^\dagger(a))]$$

which directly parallels the classical finite-dimensional setting [Vapnik, 1998]. Showing the existence of minimizers, in the infinite-dimensional setting, remains a challenging open problem. We will approach this problem in the test-train setting by using a data-driven empirical approximation to the cost used to determine θ and to test the accuracy of the approximation. Because we conceptualize our methodology in the infinite-dimensional setting, all finite-dimensional approximations share a common set of parameters which are consistent in infinite dimensions. Practically this means we obtain an approximation error that is independent of the function discretization – a feature not shared by standard CNNs (see Figure 2). A table of notation is shown in the Appendix 1.

Learning the Operator. Approximating the operator G^\dagger is a different and typically much more challenging task than finding the solution $u \in \mathcal{U}$ of a PDE for a single instance of the parameter $a \in \mathcal{A}$. Most existing methods, ranging from classical finite elements, finite differences, and finite volumes to modern machine learning approaches such as physics-informed neural networks (PINNs) [Raissi et al., 2019] aim at the latter and can therefore be computationally expensive. This makes them impractical for applications where a solution to the PDE is required for many different instances of the parameter. On the other hand, our approach directly approximates the operator and is therefore much cheaper and faster, offering tremendous computational savings when compared to traditional solvers. For an example application to Bayesian inverse problems, see Section 5.4.

Discretization. Since our data a_j and u_j are, in general, functions, to work with them numerically, we assume access only to point-wise evaluations. Let $D_j = \{x_1, \dots, x_n\} \subset D$ be a n -point discretization of the domain D and assume we have observations $a_j|_{D_j} \in \mathbb{R}^{n \times d_a}$, $u_j|_{D_j} \in \mathbb{R}^{n \times d_v}$, for a finite collection of input-output pairs indexed by j . To be discretization-invariant, the neural operator can produce an answer $u(x)$ for any $x \in D$, potentially $x \notin D_j$. Such a property is highly desirable as it allows a transfer of solutions between different grid geometries and discretizations. We note that, while the application of our methodology is based on having point-wise evaluations of the function, it is not limited by it. One may, for example, represent a function numerically as a finite set of truncated basis coefficients. Invariance of the representation would then be with respect to the size of this set. Our methodology can, in principle, be modified to accommodate this scenario through a suitably chosen architecture. We do not pursue this direction in the current work.

3 Neural Operator

The neural operator, proposed in [Li et al., 2020b], is formulated as an iterative architecture $v_0 \mapsto v_1 \mapsto \dots \mapsto v_T$ where v_j for $j = 0, 1, \dots, T - 1$ is a sequence of functions each taking values in \mathbb{R}^{d_v} . The input $a \in \mathcal{A}$ is first lifted to a higher dimensional representation $v_0 = P(a)$ by the local (pointwise) transformation P which is usually parameterized by a shallow fully-connected neural network. By a local transformation we mean that $P : \mathbb{R}^{d_a} \rightarrow \mathbb{R}^{d_v}$ acts independently on each spatial component $a(x) \in \mathbb{R}^{d_a}$ of the function $a \in \mathcal{A}$. Similarly the output $u = Q(v_T)$ is the projection of v_T by the local transformation $Q : \mathbb{R}^{d_v} \rightarrow \mathbb{R}^{d_u}$. In each iteration, the update $v_t \mapsto v_{t+1}$ is defined as the composition of a non-local integral operator \mathcal{K} and a local, nonlinear activation function σ .

Definition 1 (Iterative updates) Define the update to the representation $v_t \mapsto v_{t+1}$ by

$$v_{t+1}(x) := \sigma\left(Wv_t(x) + (\mathcal{K}(a; \phi)v_t)(x)\right), \quad \forall x \in D \quad (3)$$

where $\mathcal{K} : \mathcal{A} \times \Theta_{\mathcal{K}} \rightarrow \mathcal{L}(\mathcal{U}(D; \mathbb{R}^{d_v}), \mathcal{U}(D; \mathbb{R}^{d_v}))$ maps to bounded linear operators on $\mathcal{U}(D; \mathbb{R}^{d_v})$ and is parameterized by $\phi \in \Theta_{\mathcal{K}}$, $W : \mathbb{R}^{d_v} \rightarrow \mathbb{R}^{d_v}$ is a linear transformation, and $\sigma : \mathbb{R} \rightarrow \mathbb{R}$ is a non-linear activation function whose action is defined component-wise.

We choose $\mathcal{K}(a; \phi)$ to be a kernel integral transformation parameterized by a neural network.

Definition 2 (Kernel integral operator \mathcal{K}) Define the kernel integral operator mapping in (3) by

$$(\mathcal{K}(a; \phi)v_t)(x) := \int_D \kappa(x, y, a(x), a(y); \phi)v_t(y)dy, \quad \forall x \in D \quad (4)$$

where $\kappa_\phi : \mathbb{R}^{2(d+d_a)} \rightarrow \mathbb{R}^{d_v \times d_v}$ is a neural network parameterized by $\phi \in \Theta_{\mathcal{K}}$.

Here κ_ϕ plays the role of a kernel function which we learn from data. Together definitions 1 and 2 constitute a generalization of neural networks to infinite-dimensional spaces as first proposed in [Li et al., 2020b]. If we remove the dependence on the function a and impose $\kappa_\phi(x, y) = \kappa_\phi(x - y)$, we obtain that (4) is a convolution operator. We exploit this fact in the following section by parameterizing κ_ϕ directly in Fourier space and using the Fast Fourier Transform (FFT) to efficiently compute (4). This leads to a fast architecture which obtains state-of-the-art results for PDE problems.

4 Fourier Neural Operator

We propose replacing the kernel integral operator in (4), by a convolution operator defined in Fourier space. Let \mathcal{F} denote the Fourier transform of a function $f : D \rightarrow \mathbb{R}^{d_v}$ and \mathcal{F}^{-1} its inverse then

$$(\mathcal{F}f)_j(k) = \int_D f_j(x) e^{-2i\pi(x,k)} dx, \quad (\mathcal{F}^{-1}f)_j(x) = \int_D f_j(k) e^{2i\pi(x,k)} dk$$

for $j = 1, \dots, d_v$ where $i = \sqrt{-1}$ is the imaginary unit. By letting $\kappa_\phi(x, y, a(x), a(y)) = \kappa_\phi(x - y)$ in (4) and applying the convolution theorem, we find that

$$(\mathcal{K}(a; \phi)v_t)(x) = \mathcal{F}^{-1}(\mathcal{F}(\kappa_\phi) \cdot \mathcal{F}(v_t))(x), \quad \forall x \in D.$$

We therefore propose to directly parameterize κ_ϕ in Fourier space.

Definition 3 (Fourier integral operator \mathcal{K}) Define the Fourier integral operator

$$(\mathcal{K}(\phi)v_t)(x) = \mathcal{F}^{-1}(R_\phi \cdot (\mathcal{F}v_t))(x) \quad \forall x \in D \quad (5)$$

where R_ϕ is the Fourier transform of a periodic function $\kappa : \bar{D} \rightarrow \mathbb{R}^{d_v \times d_v}$ parameterized by $\phi \in \Theta_{\mathcal{K}}$.

For frequency mode $k \in D$, we have $(\mathcal{F}v_t)(k) \in \mathbb{C}^{d_v}$ and $R_\phi(k) \in \mathbb{C}^{d_v \times d_v}$. Notice that since we assume κ is periodic, it admits a Fourier series expansion, so we may work with the discrete modes $k \in \mathbb{Z}^d$. We pick a finite-dimensional parameterization by truncating the Fourier series at a maximal number of modes $k_{\max} = |Z_{k_{\max}}| = |\{k \in \mathbb{Z}^d : |k_j| \leq k_{\max,j}, \text{ for } j = 1, \dots, d\}|$. We thus parameterize R_ϕ directly as complex-valued $(k_{\max} \times d_v \times d_v)$ -tensor comprising a collection of truncated Fourier modes and therefore drop ϕ from our notation. Since κ is real-valued, we impose conjugate symmetry. We note that the set $Z_{k_{\max}}$ is not the canonical choice for the low frequency modes of v_t . Indeed, the low frequency modes are usually defined by placing an upper-bound on the ℓ_1 -norm of $k \in \mathbb{Z}^d$. We choose $Z_{k_{\max}}$ as above since it allows for an efficient implementation.

The discrete case and the FFT. Assuming the domain D is discretized with $n \in \mathbb{N}$ points, we have that $v_t \in \mathbb{R}^{n \times d_v}$ and $\mathcal{F}(v_t) \in \mathbb{C}^{n \times d_v}$. Since we convolve v_t with a function which only has k_{\max} Fourier modes, we may simply truncate the higher modes to obtain $\mathcal{F}(v_t) \in \mathbb{C}^{k_{\max} \times d_v}$. Multiplication by the weight tensor $R \in \mathbb{C}^{k_{\max} \times d_v \times d_v}$ is then

$$(R \cdot (\mathcal{F}v_t))_{k,l} = \sum_{j=1}^{d_v} R_{k,l,j} (\mathcal{F}v_t)_{k,j}, \quad k = 1, \dots, k_{\max}, \quad j = 1, \dots, d_v. \quad (6)$$

When the discretization is uniform with resolution $s_1 \times \dots \times s_d = n$, \mathcal{F} can be replaced by the Fast Fourier Transform. For $f \in \mathbb{R}^{n \times d_v}$, $k = (k_1, \dots, k_d) \in \mathbb{Z}_{s_1} \times \dots \times \mathbb{Z}_{s_d}$, and $x = (x_1, \dots, x_d) \in D$, the FFT $\hat{\mathcal{F}}$ and its inverse $\hat{\mathcal{F}}^{-1}$ are defined as

$$\begin{aligned} (\hat{\mathcal{F}}f)_l(k) &= \sum_{x_1=0}^{s_1-1} \dots \sum_{x_d=0}^{s_d-1} f_l(x_1, \dots, x_d) e^{-2i\pi \sum_{j=1}^d \frac{x_j k_j}{s_j}}, \\ (\hat{\mathcal{F}}^{-1}f)_l(x) &= \sum_{k_1=0}^{s_1-1} \dots \sum_{k_d=0}^{s_d-1} f_l(k_1, \dots, k_d) e^{2i\pi \sum_{j=1}^d \frac{x_j k_j}{s_j}} \end{aligned}$$

for $l = 1, \dots, d_v$. where we abuse notation and index the rows of the matrix f by either the Fourier mode k or the spatial location x and index the column by the subscript l . In this case, the set of truncated modes becomes

$$Z_{k_{\max}} = \{(k_1, \dots, k_d) \in \mathbb{Z}_{s_1} \times \dots \times \mathbb{Z}_{s_d} \mid k_j \leq k_{\max,j} \text{ or } s_j - k_j \leq k_{\max,j}, \text{ for } j = 1, \dots, d\}.$$

When implemented, R is treated as a $(s_1 \times \dots \times s_d \times d_v \times d_v)$ -tensor and the above definition of $Z_{k_{\max}}$ corresponds to the ‘‘corners’’ of R , which allows for a straight-forward parallel implementation of (6) via matrix-vector multiplication. In practice, we have found that choosing $k_{\max,j} = 12$ which yields $k_{\max} = 12^d$ parameters per channel to be sufficient for all the task that we consider.

Parameterizations of R . In general, R can be defined to depend on $(\mathcal{F}a)$ to parallel (4). Indeed, we can define $R_\phi : \mathbb{Z}^d \times \mathbb{R}^{d_v} \rightarrow \mathbb{R}^{d_v \times d_v}$ as a parametric function which maps $(k, (\mathcal{F}a)(k))$ to the values of the appropriate Fourier modes. We have experimented with linear as well as neural network parameterizations of R_ϕ . We find that the linear parameterization has a similar performance to the previously described direct parameterization, while neural networks have worse performance. This is likely due to the discrete structure of the space \mathbb{Z}^d . Generally, we find that the influence of the direct dependence on a is problem dependent. Indeed, when a is an initial condition, for example in the problems presented in Sections 5.1 and 5.3, a direct dependence is unnecessary, while, when it is a geometric parameter such as in the problem presented in Section 5.2, it may be beneficial. Our experiments in this work focus on the direct parameterization presented above.

Invariance to discretization. The proposed Fourier layers are discretization-invariant, because they can learn from and evaluate functions which are discretized in an arbitrary way. Since parameters are learned directly in Fourier space, resolving the functions in physical space simply amounts to projecting on the basis $e^{2\pi i \langle x, k \rangle}$ which are well-defined everywhere on \mathbb{R}^d . This allows us to achieve super-resolution as shown in Section 5.3. Furthermore, since there is a well-defined limit as $k_{\max} \rightarrow \infty$, our architecture has a consistent error at any resolution of the inputs and outputs. On the other hand, notice that, in Figure 2, the standard CNN methods we compare against have an error which grows with the resolution.

Quasi-linear complexity. The weight tensor R contains $k_{\max} < n$ modes, so the inner multiplication has complexity $O(k_{\max})$. Therefore, the majority of the computational cost lies in computing the Fourier transform $\mathcal{F}(v_t)$ and its inverse. General Fourier transforms have complexity $O(n^2)$, however, since we truncate the series the complexity is in fact $O(nk_{\max})$, while the FFT has complexity $O(n \log n)$. Generally, we have found using FFTs to be very efficient, however a uniform discretization if required.

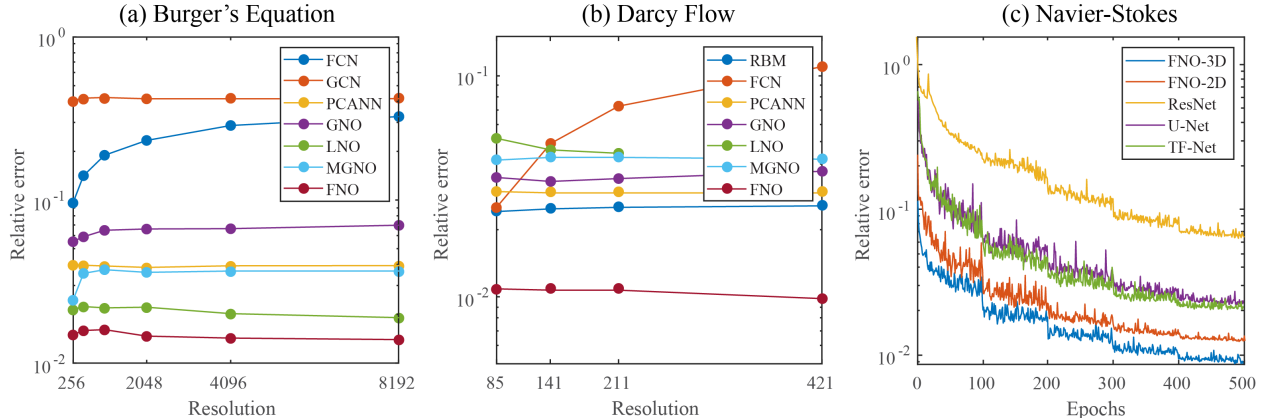
5 Numerical experiments

In this section, we compare the proposed Fourier neural operator with multiple finite-dimensional architectures as well as operator-based approximation methods on the 1-d Burgers’ equation, the 2-d Darcy Flow problem, and 2-d Navier-Stokes equation. We do not compare against traditional solvers (FEM/FDM) or neural-FEM type methods since our goal is to produce an efficient operator approximation that can be used for downstream applications. We demonstrate one such application to Bayesian inverse problem in Section 5.4.

We construct our Fourier neural operator by stacking four Fourier integral operator layers as specified in (3) and (5) with the ReLU activation as well as batch normalization. Unless otherwise specified, we use $N = 1000$ training instances and 200 testing instances. We use Adam optimizer to train for 500 epochs with an initial learning rate of 0.001 that is halved every 100 epochs. We set $k_{\max, j} = 16, d_v = 64$ for the 1-d problem and $k_{\max, j} = 12, d_v = 32$ for the 2-d problems. Lower resolution data are downsampled from higher resolution.

Spectral analysis. Due to the way we parameterize R_ϕ , the function output by (5) has at most $k_{\max, j}$ Fourier modes per channel. This, however, does not mean that the Fourier neural operator can only approximate functions up to $k_{\max, j}$ modes. Indeed, the activation functions which occur between integral operators as well as the final decoder network recover the high frequency modes. As an example, consider a solution to the Navier-Stokes equation with viscosity $\nu = 1e-3$. Truncating this function at 20 Fourier modes yields an error around 2% as shown in Figure 4 (Appendix A.2), while our Fourier neural operator learns the parametric dependence and produces approximations to an error of $\leq 1\%$ with only $k_{\max, j} = 12$ parameterized modes.

Remark on Resolution. Traditional PDE solvers such as FEM and FDM approximate a single function and therefore their error to the continuum decreases as resolution is increased. On the other hand, operator approximation is independent of the ways its data is discretized as long as all relevant information is resolved.



Left: benchmarks on Burgers equation for different resolutions; **Mid:** benchmarks on Darcy Flow for different resolutions; **Right:** the learning curves on Navier-Stokes $\nu = 1e-3$ with different benchmarks.

For acronyms, see Section 5; details in Tables 3, 1, 2.

Figure 2: Benchmark on Burger’s equation, Darcy Flow, and Navier-Stokes equation

Therefore, if we truly approximate an operator mapping, the error will be constant at any resolution of the data which our method does indeed achieve as shown in Figure 2.

Benchmarks for time-independent problems (Burgers and Darcy): **NN:** a simple point-wise feed-forward neural network. **RBM:** the classical Reduced Basis Method (using a POD basis) [DeVore, 2014]. **FCN:** a the-state-of-the-art neural network architecture based on Fully Convolution Networks [Zhu and Zabarar, 2018]. **PCANN:** an operator method using PCA as an autoencoder on both the input and output data and interpolating the latent spaces with a neural network [Bhattacharya et al., 2020]. **GNO:** the original graph neural operator [Li et al., 2020b]. **MGNO:** the multipole graph neural operator [Li et al., 2020a]. **LNO:** a neural operator method based on the low-rank decomposition of the kernel $\kappa(x, y) := \sum_{j=1}^r \phi_j(x)\psi_j(y)$, similar to the unstacked DeepONet proposed in [Lu et al., 2019]. **FNO:** the newly purposed Fourier neural operator.

Benchmarks for time-dependent problems (Navier-Stokes): **ResNet:** 18 layers of 2-d convolution with residual connections [He et al., 2016]. **U-Net:** A popular choice for image-to-image regression tasks consisting of four blocks with 2-d convolutions and deconvolutions [Ronneberger et al., 2015]. **TF-Net:** A network designed for learning turbulent flows based on a combination of spatial and temporal convolutions [Wang et al., 2020]. **FNO-2d:** 2-d Fourier neural operator with a RNN structure in time. **FNO-3d:** 3-d Fourier neural operator that directly convolves in space-time.

5.1 Burgers’ Equation

The 1-d Burgers’ equation is a non-linear PDE with various applications including modeling the one dimensional flow of a viscous fluid. It takes the form

$$\begin{aligned} \partial_t u(x, t) + \partial_x(u^2(x, t)/2) &= \nu \partial_{xx} u(x, t), & x \in (0, 1), t \in (0, 1] \\ u(x, 0) &= u_0(x), & x \in (0, 1) \end{aligned} \tag{7}$$

with periodic boundary conditions where $u_0 \in L^2_{\text{per}}((0, 1); \mathbb{R})$ is the initial condition and $\nu \in \mathbb{R}_+$ is the viscosity coefficient. We aim to learn the operator mapping the initial condition to the solution at time one, $G^\dagger : L^2_{\text{per}}((0, 1); \mathbb{R}) \rightarrow H^r_{\text{per}}((0, 1); \mathbb{R})$ defined by $u_0 \mapsto u(\cdot, 1)$ for any $r > 0$.

The initial condition $u_0(x)$ is generated according to $u_0 \sim \mu$ where $\mu = \mathcal{N}(0, 625(-\Delta + 25I)^{-2})$ with periodic boundary conditions. We set the viscosity to $\nu = 0.1$ and solve the equation using a split step method where the heat equation part is solved exactly in Fourier space then the non-linear part is advanced,

again in Fourier space, using a very fine forward Euler method. We solve on a spatial mesh with resolution $2^{13} = 8192$ and use this dataset to subsample other resolutions.

Table 1: Benchmarks on 1-d Burgers' equation

Networks	$s = 256$	$s = 512$	$s = 1024$	$s = 2048$	$s = 4096$	$s = 8192$
NN	0.4714	0.4561	0.4803	0.4645	0.4779	0.4452
GCN	0.3999	0.4138	0.4176	0.4157	0.4191	0.4198
FCN	0.0958	0.1407	0.1877	0.2313	0.2855	0.3238
PCANN	0.0398	0.0395	0.0391	0.0383	0.0392	0.0393
GNO	0.0555	0.0594	0.0651	0.0663	0.0666	0.0699
LNO	0.0212	0.0221	0.0217	0.0219	0.0200	0.0189
MGNO	0.0243	0.0355	0.0374	0.0360	0.0364	0.0364
FNO	0.0149	0.0158	0.0160	0.0146	0.0142	0.0139

The results of our experiments are shown in Figure 2 (a) and Table 1. Our proposed method obtains the lowest relative error compared to any of the benchmarks. Further, the error is invariant with the resolution, while the error of convolution neural network based methods (FCN) grows with the resolution. Compared to other neural operator methods such as GNO and MGNO that use Nyström sampling in physical space, the Fourier neural operator is both more accurate and more computationally efficient.

5.2 Darcy Flow

We consider the steady-state of the 2-d Darcy Flow equation on the unit box which is the second order, linear, elliptic PDE

$$\begin{aligned} -\nabla \cdot (a(x)\nabla u(x)) &= f(x) & x \in (0, 1)^2 \\ u(x) &= 0 & x \in \partial(0, 1)^2 \end{aligned} \tag{8}$$

with a Dirichlet boundary where $a \in L^\infty((0, 1)^2; \mathbb{R}_+)$ is the diffusion coefficient and $f \in L^2((0, 1)^2; \mathbb{R})$ is the forcing function. This PDE has numerous applications including modeling the pressure of subsurface flow, the deformation of linearly elastic materials, and the electric potential in conductive materials. We are interested in learning the operator mapping the diffusion coefficient to the solution, $G^\dagger : L^\infty((0, 1)^2; \mathbb{R}_+) \rightarrow H_0^1((0, 1)^2; \mathbb{R}_+)$ defined by $a \mapsto u$. Note that although the PDE is linear, the operator G^\dagger is not.

The coefficients $a(x)$ are generated according to $a \sim \mu$ where $\mu = \psi_\# \mathcal{N}(0, (-\Delta + 9I)^{-2})$ with zero Neumann boundary conditions on the Laplacian. The mapping $\psi : \mathbb{R} \rightarrow \mathbb{R}$ takes the value 12 on the positive part of the real line and 3 on the negative and the push-forward is defined pointwise. The forcing is kept fixed $f(x) = 1$. Such constructions are prototypical models for many physical systems such as permeability in subsurface flows and material microstructures in elasticity. Solutions u are obtained by using a second-order finite difference scheme on a 421×421 grid. Different resolutions are downsampled from this dataset.

The results of our experiments are shown in Figure 2 (b) and Table 2. The proposed Fourier neural operator obtains nearly one order of magnitude lower relative error compared any benchmarks. We again observe the invariance of the error with respect to the resolution.

5.3 Navier-Stoke

We consider the 2-d Navier-Stokes equation for a viscous, incompressible fluid in vorticity form on the unit torus:

$$\begin{aligned} \partial_t w(x, t) + u(x, t) \cdot \nabla w(x, t) &= \nu \Delta w(x, t) + f(x), & x \in (0, 1)^2, t \in (0, T] \\ \nabla \cdot u(x, t) &= 0, & x \in (0, 1)^2, t \in [0, T] \\ w(x, 0) &= w_0(x), & x \in (0, 1)^2 \end{aligned} \tag{9}$$

Table 2: Benchmarks on 2-d Darcy Flow

Networks	$s = 85$	$s = 141$	$s = 211$	$s = 421$
NN	0.1716	0.1716	0.1716	0.1716
FCN	0.0253	0.0493	0.0727	0.1097
PCANN	0.0299	0.0298	0.0298	0.0299
RBM	0.0244	0.0251	0.0255	0.0259
GNO	0.0346	0.0332	0.0342	0.0369
LNO	0.0520	0.0461	0.0445	–
MGNO	0.0416	0.0428	0.0428	0.0420
FNO	0.0108	0.0109	0.0109	0.0098

where $u \in C([0, T]; H_{\text{per}}^r((0, 1)^2; \mathbb{R}^2))$ for any $r > 0$ is the velocity field, $w = \nabla \times u$ is the vorticity, $w_0 \in L_{\text{per}}^2((0, 1)^2; \mathbb{R})$ is the initial vorticity, $\nu \in \mathbb{R}_+$ is the viscosity coefficient, and $f \in L_{\text{per}}^2((0, 1)^2; \mathbb{R})$ is the forcing function. We are interested in learning the operator mapping the vorticity up to time 10 to the vorticity up to some later time $T > 10$, $G^\dagger : C([0, 10]; H_{\text{per}}^r((0, 1)^2; \mathbb{R})) \rightarrow C([10, T]; H_{\text{per}}^r((0, 1)^2; \mathbb{R}))$ defined by $w|_{(0, 1)^2 \times [0, 10]} \mapsto w|_{(0, 1)^2 \times [10, T]}$. We experiment with the viscosities $\nu = 1\text{e-}3, 1\text{e-}4, 1\text{e-}5$, decreasing the final time T as the dynamic becomes chaotic.

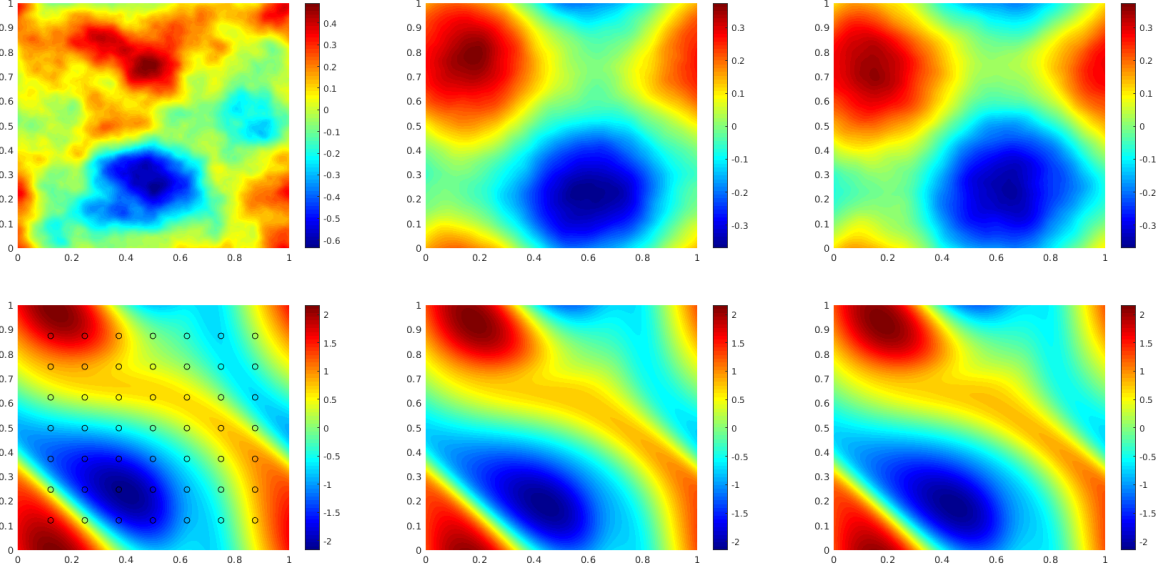
The initial condition $w_0(x)$ is generated according to $w_0 \sim \mu$ where $\mu = \mathcal{N}(0, 7^{3/2}(-\Delta + 49I)^{-2.5})$ with periodic boundary conditions. The forcing is kept fixed $f(x) = 0.1(\sin(2\pi(x_1 + x_2)) + \cos(2\pi(x_1 + x_2)))$. The equation is solved using the stream-function formulation with a pseudospectral method. First a Poisson equation is solved in Fourier space to find the velocity field. Then the vorticity is differentiated and the non-linear term is computed in physical space after which it is dealiased. Time is advanced with a Crank–Nicolson update where the non-linear term does not enter the implicit part. All data are generated on a 256×256 grid and are downsampled to 64×64 . We use a time-step of $1\text{e-}4$ for the Crank–Nicolson scheme in the data-generated process where we record the solution every $t = 1$ time units. The step is increased to $2\text{e-}2$ when used in MCMC for the Bayesian inverse problem.

Table 3: Benchmarks on Navier Stokes

Config	Parameters	Time per epoch	$\nu = 1\text{e-}3$	$\nu = 1\text{e-}4$	$\nu = 1\text{e-}4$	$\nu = 1\text{e-}5$
			$T = 50$ $N = 1000$	$T = 30$ $N = 1000$	$T = 30$ $N = 10000$	$T = 20$ $N = 1000$
FNO-3D	6, 558, 537	38.99s	0.0086	0.1918	0.0820	0.1893
FNO-2D	414, 517	127.80s	0.0128	0.1559	0.0973	0.1556
U-Net	24, 950, 491	48.67s	0.0245	0.2051	0.1190	0.1982
TF-Net	7, 451, 724	47.21s	0.0225	0.2253	0.1168	0.2268
ResNet	266, 641	78.47s	0.0701	0.2871	0.2311	0.2753

As shown in Table 3, the FNO-3D has the best performance when there is sufficient data ($\nu = 1\text{e-}3, N = 1000$ and $\nu = 1\text{e-}4, N = 10000$). For the configurations where the amount of data is insufficient ($\nu = 1\text{e-}4, N = 1000$ and $\nu = 1\text{e-}5, N = 1000$), all methods have $> 15\%$ error with FNO-2D achieving the lowest. Note that we only present results for spatial resolution 64×64 since all benchmarks we compare against are designed for this resolution. Increasing it degrades their performance while FNO achieves the same errors as in Table 3.

2-d and 3-d Convolutions. FNO-2D, U-Net, TF-Net, and ResNet all use 2D-convolution in the spatial domain and recurrently propagate in the time domain (2D+RNN). On the other hand, FNO-3D performs convolution in space-time. The Conv2D+RNN structure can propagate the solution to any arbitrary time T



The top left panel shows the true initial vorticity while bottom left panel shows the true observed vorticity at $T = 50$ with black dots indicating the locations of the observation points placed on a 7×7 grid. The top middle panel shows the posterior mean of the initial vorticity given the noisy observations estimated with MCMC using the traditional solver, while the top right panel shows the same thing but using FNO as a surrogate model. The bottom middle and right panels show the vorticity at $T = 50$ when the respective approximate posterior means are used as initial conditions.

Figure 3: Results of the Bayesian inverse problem for the Navier-Stokes equation.

in increments of a fixed interval length Δt , while the Conv3D structure is fixed to the interval $[0, T]$ but can transfer the solution to an arbitrary time-discretization. Figure 1 shows an example where we train FNO-3D on $64 \times 64 \times 20$ data and transfer to $256 \times 256 \times 80$, demonstrating super-resolution in space-time. We find the 3-d method to be more expressive and easier to train compared to its RNN-structured counterpart.

5.4 Bayesian Inverse Problem.

In this experiment, we use a function space Markov chain Monte Carlo (MCMC) method [Cotter et al., 2013] to draw samples from the posterior distribution of the initial vorticity in Navier-Stokes given sparse, noisy observations at time $T = 50$. We compare the Fourier neural operator acting as a surrogate model with the traditional solvers used to generate our train-test data (both run on GPU). We generate 25,000 samples from the posterior (with a 5,000 sample burn-in period), requiring 30,000 evaluations of the forward operator.

As shown in Figure 3, FNO and the traditional solver recover almost the same posterior mean which, when pushed forward, recovers well the late-time dynamic of Navier Stokes. In a sharp contrast, FNO takes 0.005s to evaluate a single instances while the traditional solver, after being optimized to use the largest possible internal time-step which does not lead to blow-up, takes 2.2s. This amounts to 2.5 minutes for the MCMC using FNO and over 18 hours for the traditional solver. Even if we account for data generation and training time (offline steps) which take 12 hours, using FNO is still faster! Once trained, FNO can be used to quickly perform multiple MCMC runs for different initial conditions and observations, while the traditional solver will take 18 hours for every instance. It is because data-driven method such as FNO does not require roll-out in time; it has 4 Fourier layers in total, while the traditional solver need to have a time step $\Delta t = 0.01$ to maintain a reasonable accuracy. The speed advantage could attribute to better parallelization of deep learning methods on GPU. Furthermore, since FNO is differentiable, it can easily be applied to PDE-constrained optimization problems without need for the adjoint method.

6 Discussion and Conclusion

Activation functions on the spatial domain. We choose to apply the activation functions on the spatial domain. One can instead directly apply activation functions on the Fourier domain. But in practice, it doesn't work as well, because the pointwise activation function in the Fourier domain is equivalent to spatial convolution, which loses the meaning of the activation functions. We need the activation functions on the spatial domain to recover the higher Fourier modes and non-periodic boundary condition.

Periodic boundary condition. Traditional Fourier methods work only with periodic boundary conditions, however, our Fourier neural operator does not have this limitation (Darcy and the time domain of Navier-Stokes). This is due to the final decoder network which is able to learn the right boundary condition.

Recurrent structure. The neural operator has an iterative structure that can naturally be formulated as a recurrent network where all layers share the same parameters without sacrificing performance. We observe that this is not the case for convolutional networks.

Computer vision. Operator learning is not restricted to PDEs. Images can naturally be viewed as real-valued functions on 2-d domains and videos simply add a temporal structure. Our approach is therefore a natural choice for problems in computer vision where invariance to discretization crucial. We leave this as an interesting and exciting future direction.

Acknowledgements

Z. Li gratefully acknowledges the financial support from the Kortschak Scholars Program. A. Anandkumar is supported in part by Bren endowed chair, LwLL grants, Beyond Limits, Raytheon, Microsoft, Google, Adobe faculty fellowships, and DE Logi grant. K. Bhattacharya, N. B. Kovachki, B. Liu and A. M. Stuart gratefully acknowledge the financial support of the Army Research Laboratory through the Cooperative Agreement Number W911NF-12-0022. Research was sponsored by the Army Research Laboratory and was accomplished under Cooperative Agreement Number W911NF-12-2-0022. The views and conclusions contained in this document are those of the authors and should not be interpreted as representing the official policies, either expressed or implied, of the Army Research Laboratory or the U.S. Government. The U.S. Government is authorized to reproduce and distribute reprints for Government purposes notwithstanding any copyright notation herein.

References

- [Adler and Oktem, 2017] Adler, J. and Oktem, O. (2017). Solving ill-posed inverse problems using iterative deep neural networks. *Inverse Problems*.
- [Bar and Sochen, 2019] Bar, L. and Sochen, N. (2019). Unsupervised deep learning algorithm for pde-based forward and inverse problems. *arXiv preprint arXiv:1904.05417*.
- [Bengio et al., 2007] Bengio, Y., LeCun, Y., et al. (2007). Scaling learning algorithms towards ai. *Large-scale kernel machines*, 34(5):1–41.
- [Bhatnagar et al., 2019] Bhatnagar, S., Afshar, Y., Pan, S., Duraisamy, K., and Kaushik, S. (2019). Prediction of aerodynamic flow fields using convolutional neural networks. *Computational Mechanics*, pages 1–21.
- [Bhattacharya et al., 2020] Bhattacharya, K., Kovachki, N. B., and Stuart, A. M. (2020). Model reduction and neural networks for parametric pde(s). *preprint*.
- [Cotter et al., 2013] Cotter, S. L., Roberts, G. O., Stuart, A. M., and White, D. (2013). Mcmc methods for functions: Modifying old algorithms to make them faster. *Statistical Science*, 28(3):424–446.

- [DeVore, 2014] DeVore, R. A. (2014). *Chapter 3: The Theoretical Foundation of Reduced Basis Methods*.
- [E and Yu, 2018] E, W. and Yu, B. (2018). The deep ritz method: A deep learning-based numerical algorithm for solving variational problems. *Communications in Mathematics and Statistics*.
- [Fan et al., 2019a] Fan, Y., Bohorquez, C. O., and Ying, L. (2019a). Bcr-net: A neural network based on the nonstandard wavelet form. *Journal of Computational Physics*, 384:1–15.
- [Fan et al., 2019b] Fan, Y., Lin, L., Ying, L., and Zepeda-Núñez, L. (2019b). A multiscale neural network based on hierarchical matrices. *Multiscale Modeling & Simulation*, 17(4):1189–1213.
- [Guo et al., 2016] Guo, X., Li, W., and Iorio, F. (2016). Convolutional neural networks for steady flow approximation. In *Proceedings of the 22nd ACM SIGKDD International Conference on Knowledge Discovery and Data Mining*.
- [He et al., 2016] He, K., Zhang, X., Ren, S., and Sun, J. (2016). Deep residual learning for image recognition. In *Proceedings of the IEEE conference on computer vision and pattern recognition*, pages 770–778.
- [Hornik et al., 1989] Hornik, K., Stinchcombe, M., White, H., et al. (1989). Multilayer feedforward networks are universal approximators. *Neural networks*, 2(5):359–366.
- [Khoo et al., 2017] Khoo, Y., Lu, J., and Ying, L. (2017). Solving parametric PDE problems with artificial neural networks. *arXiv preprint arXiv:1707.03351*.
- [Li et al., 2020a] Li, Z., Kovachki, N., Azizzadenesheli, K., Liu, B., Bhattacharya, K., Stuart, A., and Anandkumar, A. (2020a). Multipole graph neural operator for parametric partial differential equations.
- [Li et al., 2020b] Li, Z., Kovachki, N., Azizzadenesheli, K., Liu, B., Bhattacharya, K., Stuart, A., and Anandkumar, A. (2020b). Neural operator: Graph kernel network for partial differential equations. *arXiv preprint arXiv:2003.03485*.
- [Lu et al., 2019] Lu, L., Jin, P., and Karniadakis, G. E. (2019). Deeponet: Learning nonlinear operators for identifying differential equations based on the universal approximation theorem of operators. *arXiv preprint arXiv:1910.03193*.
- [Mathieu et al., 2013] Mathieu, M., Henaff, M., and LeCun, Y. (2013). Fast training of convolutional networks through ffts.
- [Mingo et al., 2004] Mingo, L., Aslanyan, L., Castellanos, J., Diaz, M., and Riazanov, V. (2004). Fourier neural networks: An approach with sinusoidal activation functions.
- [Nelsen and Stuart, 2020] Nelsen, N. and Stuart, A. (2020). The random feature model for input-output maps between banach spaces. *arXiv preprint arXiv:2005.10224*.
- [Raissi et al., 2019] Raissi, M., Perdikaris, P., and Karniadakis, G. E. (2019). Physics-informed neural networks: A deep learning framework for solving forward and inverse problems involving nonlinear partial differential equations. *Journal of Computational Physics*, 378:686–707.
- [Ronneberger et al., 2015] Ronneberger, O., Fischer, P., and Brox, T. (2015). U-net: Convolutional networks for biomedical image segmentation. In *International Conference on Medical image computing and computer-assisted intervention*, pages 234–241. Springer.
- [Sitzmann et al., 2020] Sitzmann, V., Martel, J. N., Bergman, A. W., Lindell, D. B., and Wetzstein, G. (2020). Implicit neural representations with periodic activation functions. *arXiv preprint arXiv:2006.09661*.
- [Smith et al., 2020] Smith, J. D., Azizzadenesheli, K., and Ross, Z. E. (2020). Eikonet: Solving the eikonal equation with deep neural networks. *arXiv preprint arXiv:2004.00361*.
- [Vapnik, 1998] Vapnik, V. N. (1998). *Statistical Learning Theory*. Wiley-Interscience.

- [Wang et al., 2020] Wang, R., Kashinath, K., Mustafa, M., Albert, A., and Yu, R. (2020). Towards physics-informed deep learning for turbulent flow prediction. In *Proceedings of the 26th ACM SIGKDD International Conference on Knowledge Discovery & Data Mining*, pages 1457–1466.
- [Zhu and Zabaras, 2018] Zhu, Y. and Zabaras, N. (2018). Bayesian deep convolutional encoder–decoder networks for surrogate modeling and uncertainty quantification. *Journal of Computational Physics*.

A Appendix

A.1 Table of notations

A table of notations is given in Table 4.

Table 4: table of notations

Notation	Meaning
Operator learning	
$D \subset \mathbb{R}^d$	The spatial domain for the PDE
$x \in D$	Points in the the spatial domain
$a \in \mathcal{A} = (D; \mathbb{R}^{d_a})$	The input coefficient functions
$u \in \mathcal{U} = (D; \mathbb{R}^{d_u})$	The target solution functions
D_j	The discretization of (a_j, u_j)
$G^\dagger : \mathcal{A} \rightarrow \mathcal{U}$	The operator mapping the coefficients to the solutions
μ	A probability measure where a_j sampled from.
Neural operator	
$v(x) \in \mathbb{R}^{d_v}$	The neural network representation of $u(x)$
d_a	Dimension of the input $a(x)$.
d_u	Dimension of the output $u(x)$.
d_v	The dimension of the representation $v(x)$
$\kappa : \mathbb{R}^{2(d+1)} \rightarrow \mathbb{R}^{d_v \times d_v}$	The kernel maps $(x, y, a(x), a(y))$ to a $d_v \times d_v$ matrix
ϕ	The parameters of the kernel network κ
$t = 0, \dots, T$	The time steps (layers)
σ	The activation function
Fourier operator	
$\mathcal{F}, \mathcal{F}^{-1}$	Fourier transformation and its inverse.
R	The linear transformation applied on the lower Fourier modes.
W	The applied on the spatial domain.
k	Fourier modes / wave numbers.
k_{max}	The max Fourier modes used in the Fourier layer.
Hyperparameters	
N	The number of training pairs.
n	The size of the discretization.
s	The resolution of the discretization ($s^d = n$).
ν	The viscosity.
T	The time interval $[0, T]$ for time-dependent equation.

A.2 Spectral Analysis

The spectral decay of Burgers' equation, Darcy Flow, and Navier Stokes equation are shown in Figure 4. We note the harder equations with lower viscosity decay slower than others..

A.3 Data generation

In this section, we provide the details of data generator for the three equation we used in Section 5.

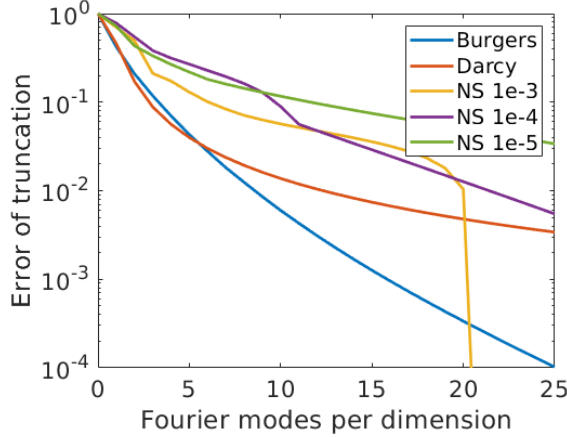


Figure 4: Spectral Decay of different equations

A.3.1 Burgers Equation

Recall the 1-d Burger's equation on the unit torus:

$$\begin{aligned} \partial_t u(x, t) + \partial_x(u^2(x, t)/2) &= \nu \partial_{xx} u(x, t), & x \in (0, 1), t \in (0, 1] \\ u(x, 0) &= u_0(x), & x \in (0, 1). \end{aligned}$$

The initial condition $u_0(x)$ is generated according to $u_0 \sim \mu$ where $\mu = \mathcal{N}(0, 625(-\Delta + 25I)^{-2})$ with periodic boundary conditions. We set the viscosity to $\nu = 0.1$ and solve the equation using a split step method where the heat equation part is solved exactly in Fourier space then the non-linear part is advanced, again in Fourier space, using a very fine forward Euler method. We solve on a spatial mesh with resolution $2^{13} = 8192$ and use this dataset to subsample other resolutions.

A.3.2 Darcy Flow

The 2-d Darcy Flow is a second order linear elliptic equation of the form

$$\begin{aligned} -\nabla \cdot (a(x)\nabla u(x)) &= f(x) & x \in (0, 1)^2 \\ u(x) &= 0 & x \in \partial(0, 1)^2. \end{aligned}$$

The coefficients $a(x)$ are generated according to $a \sim \mu$ where $\mu = \psi_{\#} \mathcal{N}(0, (-\Delta + 9I)^{-2})$ with zero Neumann boundary conditions on the Laplacian. The mapping $\psi : \mathbb{R} \rightarrow \mathbb{R}$ takes the value 12 on the positive part of the real line and 3 on the negative and the push-forward is defined pointwise. The forcing is kept fixed $f(x) = 1$. Such constructions are prototypical models for many physical systems such as permeability in subsurface flows and material microstructures in elasticity. Solutions u are obtained by using a second-order finite difference scheme on a 421×421 grid. Different resolutions are downsampled from this dataset.

A.3.3 Navier-Stokes Equation

Recall the 2-d Navier-Stokes equation for a viscous, incompressible fluid in vorticity form on the unit torus:

$$\begin{aligned} \partial_t w(x, t) + u(x, t) \cdot \nabla w(x, t) &= \nu \Delta w(x, t) + f(x), & x \in (0, 1)^2, t \in (0, T] \\ \nabla \cdot u(x, t) &= 0, & x \in (0, 1)^2, t \in [0, T] \\ w(x, 0) &= w_0(x), & x \in (0, 1)^2. \end{aligned}$$

The initial condition $w_0(x)$ is generated according to $w_0 \sim \mu$ where $\mu = \mathcal{N}(0, 7^{3/2}(-\Delta + 49I)^{-2.5})$ with periodic boundary conditions. The forcing is kept fixed $f(x) = 0.1(\sin(2\pi(x_1 + x_2)) + \cos(2\pi(x_1 + x_2)))$.

The equation is solved using the stream-function formulation with a pseudospectral method. First a Poisson equation is solved in Fourier space to find the velocity field. Then the vorticity is differentiated and the non-linear term is computed in physical space after which it is dealiased. Time is advanced with a Crank–Nicolson update where the non-linear term does not enter the implicit part. All data are generated on a 256×256 grid and are downsampled to 64×64 . We use a time-step of $1e-4$ for the Crank–Nicolson scheme in the data-generated process where we record the solution every $t = 1$ time units. The step is increased to $2e-2$ when used in MCMC for the Bayesian inverse problem.